Physica E 118 (2020) 113877

Contents lists available at ScienceDirect

Physica E: Low-dimensional Systems and Nanostructures

journal homepage: www.elsevier.com/locate/physe

Intrinsic carrier mobility of monolayer GeS and GeSe: First-principles calculation

Mei Yang [a], Shuo Cao [a], Qi You [a], Li-Bin Shi [a,*], Ping Qian [b,*]

[a] School of Mathematics and Physics, Bohai University, Liaoning, Jinzhou 121013, China
[b] Department of Physics, University of Science and Technology Beijing, Beijing 100083, China

ARTICLE INFO

Keywords:
First-principles calculation
Two-dimensional semiconductors
Intrinsic mobility
Electron–phonon coupling

ABSTRACT

Recently, novel two-dimensional (2D) semiconductors of GeS and GeSe have attracted attention due to their potential applications in future nanoelectronic devices. The carrier mobility is first calculated from deformation potential theory (DPT) based on longitudinal acoustic and optical phonon model. Three important parameters of effective mass, elastic modulus and deformation potential are analyzed. Then, the intrinsic mobility is calculated from EPC matrix element. If the polarization effect of semiconductor is considered in the calculation, the electron mobility of GeS (GeSe) is reduced to 4.07×10^1 $cm^2V^{-1}s^{-1}$ (1.48×10^2 $cm^2V^{-1}s^{-1}$) for x direction, and 1.94×10^1 $cm^2V^{-1}s^{-1}$ (7.55×10^1 $cm^2V^{-1}s^{-1}$) for y direction. The hole mobility is 4.77×10^1 $cm^2V^{-1}s^{-1}$ (2.47×10^2 $cm^2V^{-1}s^{-1}$) for x direction, and 1.52×10^1 $cm^2V^{-1}s^{-1}$ (1.16×10^2 $cm^2V^{-1}s^{-1}$) for y direction. It is found that longitudinal optical phonon scattering plays a decisive role in carrier mobility. In this study, we illustrate that DPT model from the longitudinal acoustic and optical phonon scattering will overestimate carrier mobility. Some factors that affect carrier mobility are revealed.

1. Introduction

Two-dimensional (2D) semiconductors with appropriate band gap have wide application prospects in the field of optoelectronics, such as transistors, energy converters and photodetectors [1–5]. However, their applications are limited by the carrier mobility [6–10]. The mobility characterizes the response speed of electrons or holes driven by electric field [11–13], which largely depends on the scattering process, such as defect [14,15], interface [16], and phonon scattering [17,18]. Among them, the scattering of defect can be weakened by improving sample preparation technology [19]. Interface scattering can be eliminated by 2D materials with a smooth surface [20–24]. Phonon scattering determines the intrinsic mobility, which decides whether the material itself has potential application prospects [25–29]. This requires us to find an accurate theoretical method to predict the intrinsic mobility of carriers. Traditional deformation potential theory (DPT) based on longitudinal acoustic branch is widely used to predict the intrinsic mobility of carriers because of its simple theoretical formula including three parameters of effective mass, elastic modulus and deformation potential [30–34]. However, it only considers the longitudinal acoustic branch scattering mechanism, ignores other acoustic, optical phonons [35,36] and polarization effect [37–39]. Moreover, it assumes an isotropic electron–phonon interaction [40]. Therefore, in order to obtain more accurate carrier mobility, electron–phonon coupling (EPC) matrix elements in each scattering process should be considered in the calculations. However, the calculation is extremely expensive, and only a small number of 2D materials are investigated [41].

In recent years, group-IV monochalcogenides GeS and GeSe with folded structure similar to black phosphorus [42–44] have attracted wide attention [45–49]. At present, they have been successfully synthesized by a simple solution-based method or simple one-pot solution-chemistry route [50,51]. The monolayer GeS and GeSe are indirect band gap semiconductors with thermodynamic stability [52,53], highly anisotropic behavior [54] and ideal mobility [55]. Therefore, they are expected to become ideal candidates for the nanoelectronic devices [56,57]. Previous studies have shown that the electron mobility of monolayer GeS and GeSe is 3.20×10^2–1.69×10^4 cm^2 V^{-1} s^{-1} and 3.07×10^2–4.71×10^3 cm^2 V^{-1} s^{-1} [58–62]. The hole mobility is 5.00×10^1–1.60×10^2 cm^2 V^{-1} s^{-1} and 7.60×10^1–3.23×10^2 cm^2 V^{-1} s^{-1} [58–61], respectively. It is found that the carrier mobility obtained from DPT is quite different. Furthermore, does DPT overestimate mobility? Therefore, the mobility still need to be further verified.

In this study, we systematically investigate the charge transport properties of monolayer GeS and GeSe by first principles calculation and Wannier functions interpolation. First, the carrier mobility is calculated by DPT based on the longitudinal acoustic and optical branch scattering. Then, the intrinsic mobility is calculated by EPC matrix

* Corresponding authors.
E-mail addresses: slb0813@126.com (L.-B. Shi), qianping@ustb.edu.cn (P. Qian).

https://doi.org/10.1016/j.physe.2019.113877
Received 12 November 2019; Received in revised form 2 December 2019; Accepted 9 December 2019
Available online 10 December 2019

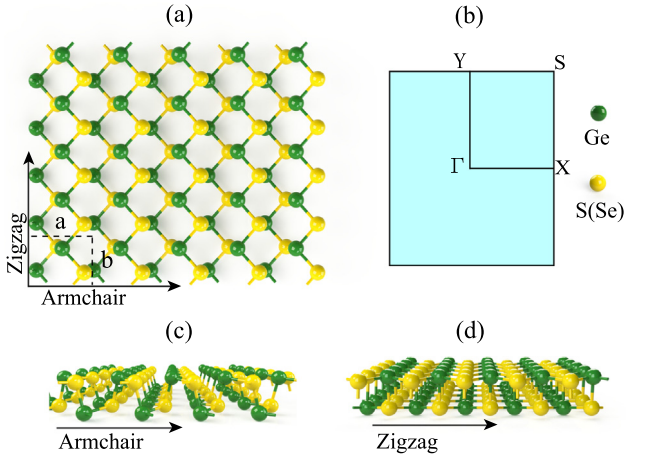

Fig. 1. (a) The atomic structure of monolayer GeS (GeSe). Dotted lines in the diagram represent their unit cell structure. Green and yellow represent Ge and S (Se) atoms, respectively. (b) The Brillouin zone and high symmetry points with Γ (0, 0), X (0.5, 0), S (0.5, 0.5) and Y (0, 0.5). (c) and (d) show their side views along armchair and zigzag directions, respectively.

elements. Finally, the effect of polarization characteristic on mobility is explained, and the factors affecting the intrinsic mobility are discussed.

2. Computational details

2.1. Details on first-principles calculation

The calculation is performed based on density functional theory (DFT) with Quantum Espresso package (QE) [63]. The Norm-conserving pseudopotentials are employed. The generalized gradient approximation (GGA) [64] with Perdew Burke Ernzerhof (PBE) [65] is used for exchange–correlation functional. In order to eliminate inter-layer interaction, a vacuum region along z direction with the thickness of 15 Å is established. The energy cutoffs for plane wave functional and charge density are set to 650 and 2600 eV, respectively, which are accurate enough to describe the valence electron configurations of Ge $3d^{10}4s^24p^2$, S $3s^23p^4$ and Se $4s^24p^4$. The convergence criteria of force is set to 10^{-4} eV/Å. Brillouin zone is integrated by using $10 \times 10 \times 1$ **k** coarse grids and $5 \times 5 \times 1$ **q** coarse grids.

Fig. 1 shows that monolayer GeS (GeSe) is similar to black phosphorus and belongs to the same orthorhombic crystal system. There are two special directions: armchair and zigzag directions. The armchair direction has hinged structure similar to black phosphorus. The structural anisotropy may lead to different charge transport properties, which will be discussed later. We define x axis parallel to the armchair direction, and y axis to the zigzag direction. The lattice and atom are completely relaxed until convergence. The optimized lattice constants for monolayer GeS (GeSe) are a = 4.43 Å and b = 3.67 Å (a = 4.27 Å and b = 3.97 Å), which are close to the experimental values of a = 4.30 Å and b = 3.64 Å (a = 4.29 Å and b = 3.97 Å) [66,67].

2.2. Carrier mobility obtained from longitudinal acoustic phonon DPT

The DPT based on longitudinal acoustic branch was proposed by Bardeen and Shockley [68], and has been successfully applied to the mobility of 2D semiconductors. For anisotropic 2D semiconductor, the formula can be described as [9,23,69]:

$$\mu_x = \frac{5e\hbar^3(5C_x + 3C_y)}{2k_BTm_x^{*\frac{3}{2}}m_y^{*\frac{1}{2}}(9E_x^2 + 7E_xE_y + 4E_y^2)}$$
$$\mu_y = \frac{5e\hbar^3(3C_x + 5C_y)}{2k_BTm_x^{*\frac{1}{2}}m_y^{*\frac{3}{2}}(4E_x^2 + 7E_xE_y + 9E_y^2)} \quad (1)$$

where e is the electron charge, $\hbar$ the reduced Planck constant, k_B the Boltzmann constant, T the thermodynamic temperature, m^* the effective mass, C the modulus of elasticity, and E the deformation potential.

2.3. Carrier mobility obtained from optical phonon DPT

According to the relaxation time approximation, the mobility for carrier scattered from optical phonon is given [18].

$$\mu_x = \frac{2e\hbar^2\rho\omega_\lambda}{m_x^{*\frac{3}{2}}m_y^{*\frac{1}{2}}D_{op}^2(2n_\lambda + 1)}$$
$$\mu_y = \frac{2e\hbar^2\rho\omega_\lambda}{m_x^{*\frac{1}{2}}m_y^{*\frac{3}{2}}D_{op}^2(2n_\lambda + 1)} \quad (2)$$

where ρ is the mass density of 2D materials. n_λ is the phonon occupancy for the angular frequency ω_λ and the mode λ. The phonon follows the Bose–Einstein distribution. D_{op} is the deformation potential for optical phonon scattering.

2.4. Carrier mobility from electron–phonon coupling (EPC) matrix element

Based on the relaxation time approximation, the carrier mobility formula from EPC matrix elements is obtained as follows [70]:

$$\mu_{e,\alpha\beta} = \frac{-e}{n_e\Omega}\sum_{n\in CB}\int\frac{d\boldsymbol{k}}{\Omega_{BZ}}\frac{\partial f_{n\boldsymbol{k}}}{\partial\varepsilon_{n\boldsymbol{k}}}v_{n\boldsymbol{k},\alpha}v_{n\boldsymbol{k},\beta}\tau_{n\boldsymbol{k}}$$
$$\mu_{h,\alpha\beta} = \frac{e}{n_h\Omega}\sum_{n\in VB}\int\frac{d\boldsymbol{k}}{\Omega_{BZ}}\frac{\partial(1-f_{n\boldsymbol{k}})}{\partial\varepsilon_{n\boldsymbol{k}}}v_{n\boldsymbol{k},\alpha}v_{n\boldsymbol{k},\beta}\tau_{n\boldsymbol{k}} \quad (3)$$

where n denotes the corresponding electrons or holes concentration, Ω is the volume of a unit cell, Ω_{BZ} is the volume of the first Brillouin zone, $\varepsilon_{n\boldsymbol{k}}$ and $f_{n\boldsymbol{k}}$ denote the energy level and Fermi–Dirac distribution in the equilibrium state with wave vectors $\boldsymbol{k}$ and band index n. $v_{n\boldsymbol{k},\alpha} = \hbar^{-1}\partial\varepsilon_{n\boldsymbol{k}}/\partial k_\alpha$ denotes the group velocity of the corresponding electrons or holes. $\tau_{n\boldsymbol{k}}$ is relaxation time. The calculation is performed in EPW (Electron–Phonon coupling using Wannier functions) package [71]. Electron band structure and phonon dispersion play a key role in the mobility calculation, which are exhibited in Fig. 2. The band structure and phonon dispersion obtained from DFT are the same as those from Wannier functions. Therefore, interpolation of Wannier functions provide reliability for the calculations of intrinsic mobility.

3. Results and discussion

3.1. Carrier mobility without polarization effect

3.1.1. Carrier mobility obtained from longitudinal acoustic phonon scattering

Fig. 3 shows the charge density distribution of monolayer GeS and GeSe in $3 \times 3 \times 1$ supercell. It can be seen that the electrons are mainly distributed around the S and Se atoms, indicating that Ge-S and Ge-Se display ionic bond characteristics. More electrons gather around S atoms due to strong electronegativity. To calculate carrier mobility based on longitudinal acoustic branch phonon scattering, we first investigate the electronic band structure along high-symmetry directions of monolayer GeS (GeSe). As shown in Fig. 2, the results show that monolayer GeS and GeSe are semiconductors with the indirect band gaps of 1.66 eV and 1.10 eV for GGA. Experimental measurements on GeS and GeSe nanosheets show that the band gaps are 1.58 eV and 1.14 eV [50]. It is noted from Fig. 2 that the conduction-band minimum (CBM) is between Y and Γ, the valence-band maximum (VBM) between Γ and X. For monolayer GeS, there is a local CBM′ is found to be 0.18 eV higher than CBM, and a local VBM′ 0.1 eV lower than VBM. For monolayer GeSe, local CBM′ and CBM″ is found to be 0.02 eV and 0.16 eV higher than CBM. The band structures are also investigated by

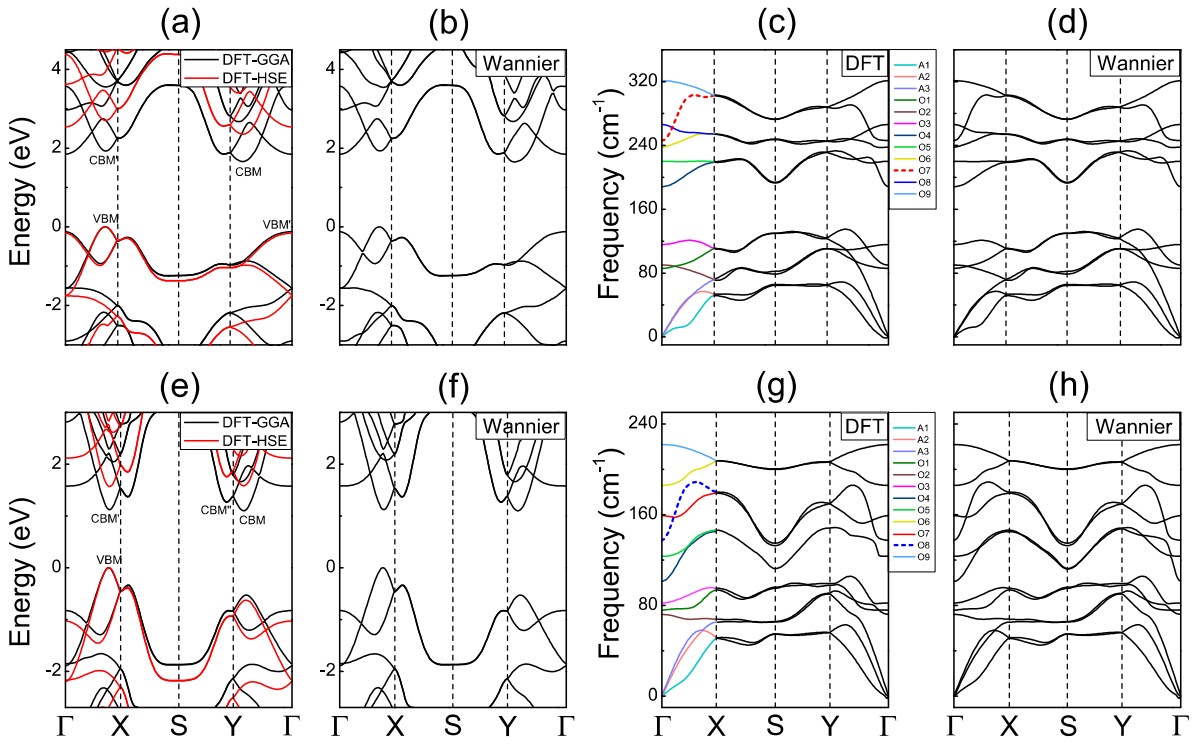

Fig. 2. The electronic band structure and phonon dispersion with (a) (b) (c) and (d) for GeS, and (e) (f) (g) and (h) for GeSe. The calculation is performed using DFT and Wannier functions interpolation, respectively. Each branch phonon mode has been identified. All phonon vibrations will be clearly given in the following work.

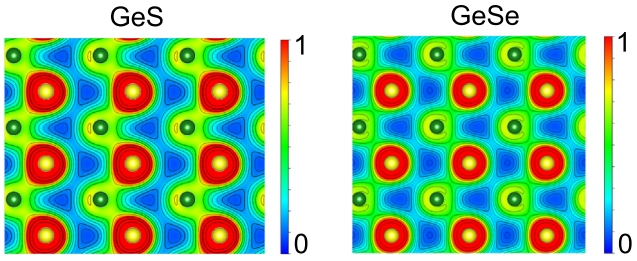

Fig. 3. The charge density distribution of monolayer GeS and GeSe. Green and yellow atoms represent Ge and S (Se), respectively.

HSE06 functional. It is noted that the shape from HSE06 is very similar to that from GGA-PBE. The band gaps of GeS and GeSe are increased to 2.36 eV and 1.57 eV, respectively.

The formula of the effective mass is $m^* = \hbar^2/(\frac{\partial E^2(\boldsymbol{k})}{\partial \boldsymbol{k}^2})$. Therefore, it can be calculated by fitting the band data near CBM and VBM with a quadratic polynomial. For monolayer GeS (GeSe), the effective mass of electrons is 0.23 m_0 (0.15 m_0) for x direction, and 0.55 m_0 (0.25 m_0) for y direction, respectively. The effective mass of holes is 0.25 m_0 (0.14 m_0) along x direction, and 0.67 m_0 (0.24 m_0) along y direction, respectively. Previous theoretical investigations on GeS (GeSe) have shown that the electron effective mass is about 0.19–0.23 m_0 (0.14–0.27 m_0) along x direction, and about 0.37–0.46 m_0 (0.25–0.30 m_0) along y direction. Hole effective mass is about 0.23–0.25 m_0 (0.15–0.16 m_0) along x direction, and about 0.59–0.87 m_0 (0.31–0.33 m_0) along y direction [58–62]. It can be seen that the effective mass in the x direction is smaller than that in the y direction, which indicates an anisotropic behavior along armchair and zigzag directions. The effective masses of carriers for CBM′, CBM″ and VBM′ are also calculated and shown in Table 1.

The elastic modulus can be regarded as a parameter to measure the elastic deformation. The higher the value, the greater the force required to produce elastic deformation, the harder the material is.

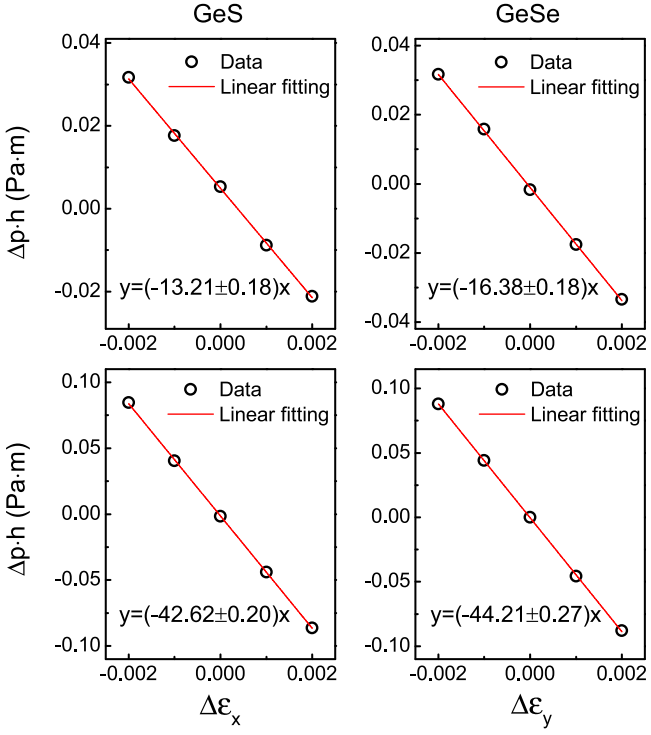

Fig. 4. Pressure multiplied by thickness versus uniaxial strain. The strain is set in the range from −0.2% to 0.2% with the interval of 0.1%. The data is fitted by a linear equation. The elastic modulus can be obtained from the slope of the fitting equation.

It can be obtained from $C = h\frac{\partial p}{\partial \varepsilon}$. As shown in Fig. 4, the elastic modulus of monolayer GeS (GeSe) is 13.21 J/m^2 (16.38 J/m^2) along x direction, and 42.62 J/m^2 (44.21 J/m^2) along y direction. The results are close to the reported values of 12.89–16.26 J/m^2 (12.11–15.92 J/m^2)

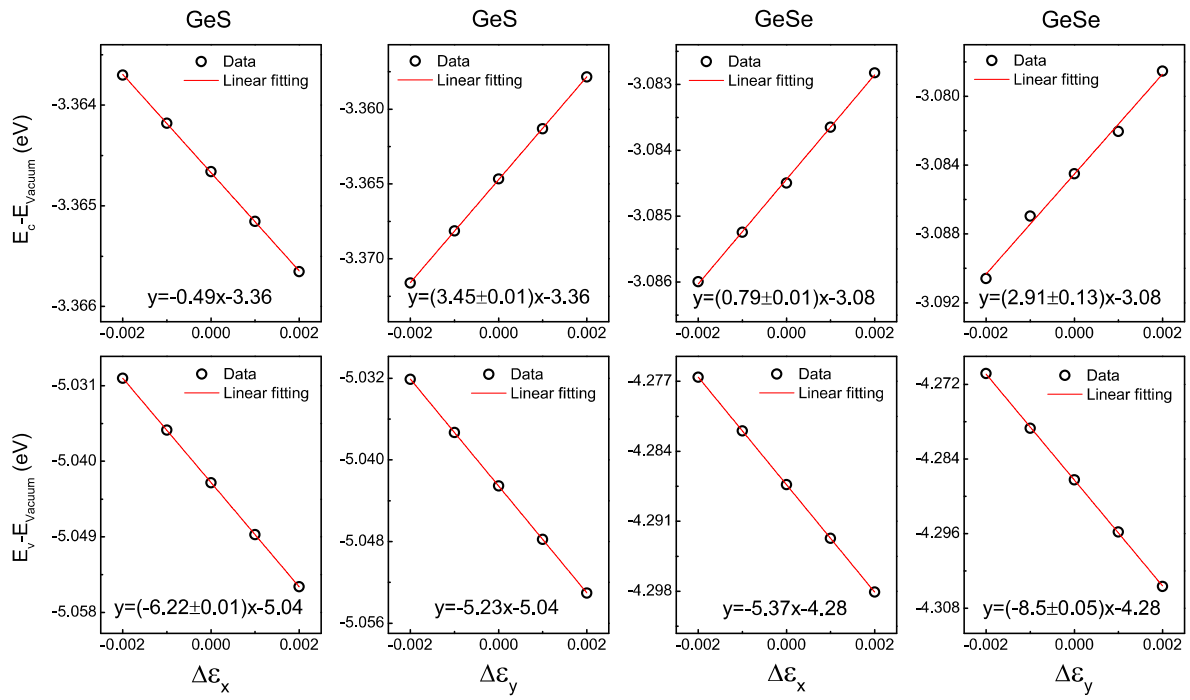

Fig. 5. Band edge versus uniaxial strain. The strain is set in the range from −0.2% to 0.2% with the interval of 0.1%. The data is fitted by a linear equation. The deformation potential is calculated from the slope of the fitting equation.

Table 1
Effective mass of carrier at VBM′, CBM′ and CBM″. Here, m_0 is electronic static mass.

Materials	Position	Carrier	m_x^*/m_0	m_y^*/m_0
GeS	CBM′	Electron	0.71	1.42
	VBM′	Hole	0.56	2.77
GeSe	CBM′	Electron	0.14	0.25
	CBM″	Electron	0.13	0.50

along x direction, and 33.40–52.37 J/m^2 (28.35–51.84 J/m^2) along y direction [58–62]. The deformation potential is calculated by the formula $E = \frac{\partial E_{edge}}{\partial \varepsilon}$. Fig. 5 shows the band edge versus uniaxial strain. In order to ensure the calculation accuracy, the uniaxial strain is set in the ranges from −0.2%~0.2% with the interval of 0.1%. The deformation potential can be obtained from the slope of linear fitting. The conduction band deformation potential is 0.49 eV (0.79 eV) along x direction, and 3.45 eV (2.91 eV) along y direction. The valence band deformation potential is 6.22 eV (5.37 eV) along x direction and 5.23 eV (8.50 eV) along y direction. Previous studies on GeS (GeSe) have shown that the conduction band deformation potential is about 0.47–2.37 eV (1.45–2.49 eV) along x direction, and about 1.73–6.13 eV (3.91–6.83 eV) along y direction. Valence band deformation potential is about 3.46–6.45 eV (2.75–5.20 eV) along x direction, and about 4.57–9.66 eV (9.67–10.01 eV) along y direction [58–62].

Based on the above three parameters of effective mass, elastic modulus and deformation potential, the carrier mobilities is presented in Table 2. For monolayer GeS, the mobility of electrons is 2.08×10^3 cm^2 V^{-1} s^{-1} along x direction, and 5.79×10^2 cm^2 V^{-1} s^{-1} along y direction, respectively. The hole mobility is 1.50×10^2 cm^2 V^{-1} s^{-1} along in x direction, and 7.94×10^1 cm^2 V^{-1} s^{-1} along y direction. For monolayer GeSe, the electron mobility is as high as 7.04×10^3 cm^2 V^{-1} s^{-1} along x direction and 3.19×10^3 cm^2 V^{-1} s^{-1} along y direction. The hole mobility is 5.08×10^2 cm^2 V^{-1} s^{-1} along x direction and 3.05×10^2 cm^2 V^{-1} s^{-1} along y direction, respectively. Because the effective mass of monolayer GeS (GeSe) in x direction is less than that in y direction, the mobilities of electrons and holes in x direction are higher than those in y direction, indicating that the GeS and GeSe exhibit an obvious anisotropy. The carriers are easier to transport in the armchair direction than in the zigzag direction.

Table 2
At room temperature (T = 300 K), electron and hole mobility obtained from longitudinal acoustic phonon DPT model in Eq. (1).

Materials	Carrier type	m^*/m_0	C (J/m^2)	E (eV)	μ (cm^2 V^{-1} s^{-1})
GeS	Electron(x)	0.23	13.21	0.49	2.08×10^3
	Electron(y)	0.55	42.62	3.45	5.79×10^2
	Hole(x)	0.25	13.21	6.22	1.50×10^2
	Hole(y)	0.67	42.62	5.23	7.94×10^1
GeSe	Electron(x)	0.15	16.38	0.79	7.04×10^3
	Electron(y)	0.25	44.21	2.91	3.19×10^3
	Hole(x)	0.14	16.38	5.37	5.08×10^2
	Hole(y)	0.24	44.21	8.5	3.05×10^2

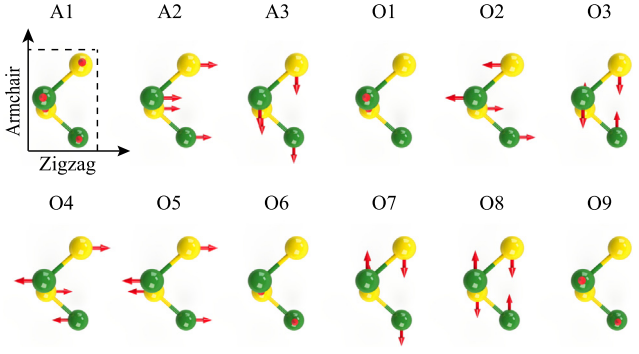

Fig. 6. The twelve phonon modes for monolayer GeS and GeSe. Arrows indicate the direction of atomic vibration.

3.1.2. Carrier mobility obtained from optical phonon scattering

Fig. 2 shows the phonon dispersion of monolayer GeS (GeSe) along high symmetric points in Brillouin zone. The unit cells of GeS and GeSe contain four atoms, thus there are twelve phonon modes including of three acoustic modes and nine optical modes. Fig. 6 exhibits the atomic vibrations corresponding to these modes. The optical phonon

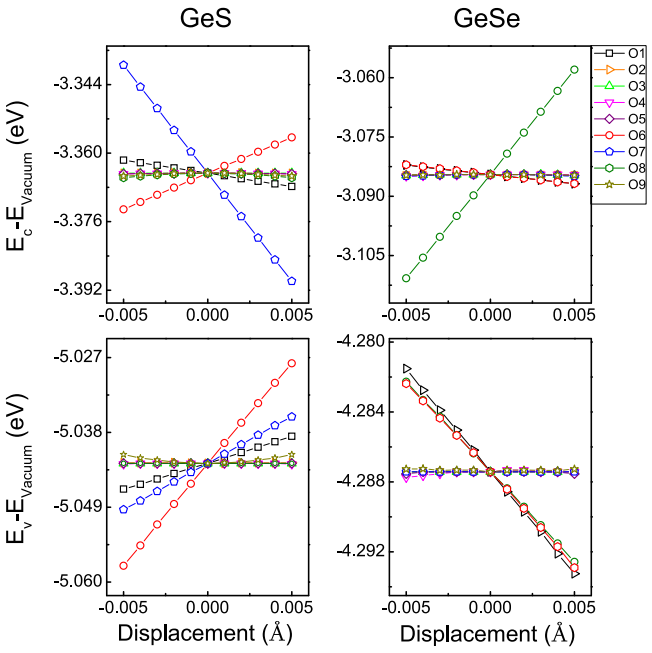

Fig. 7. Band edges versus atom displacement for monolayer GeS and GeSe. The CBM and VBM have been referred to the vacuum level. The atom displacement is set in the range from −0.005 Å to 0.005 Å with the interval of 0.001 Å. The data can be fitted by a linear equation. The deformation potential can be calculated from the slope of linear fitting curve.

Table 3
At room temperature (T = 300 K), electron and hole mobilities of monolayer GeS and GeSe obtained from optical phonon scattering.

Materials	Carrier type	μ_x (cm^2 V^{-1} s^{-1})	μ_y (cm^2 V^{-1} s^{-1})
GeS	Electron	3.85×10^2	1.60×10^2
	Hole	5.52×10^2	2.06×10^2
GeSe	Electron	5.06×10^2	3.11×10^2
	Hole	2.62×10^3	1.56×10^3

deformation potential is defined as $D_{op} = \Delta E/\Delta d$. So it can be obtained from linear fitting of band edge versus atomic displacement, as shown in Fig. 7. In this study, atomic displacement is set in the ranges from −0.005 Å to 0.005 Å with an interval of 0.001 Å. Larger conduction band deformation potentials are observed in O6 (1.68 eV/Å) and O7 (2.04 eV/Å) modes for GeS, and in O8 (5.27 eV/Å) mode for GeSe. Larger valence band deformation potential are found in O1 (0.78 eV/Å), O6 (2.98 eV/Å) and O7 (1.37 eV/Å) modes for GeS, and in O1 (1.17 eV/Å), O8 (1.03 eV/Å) and O6 (1.05 eV/Å) modes for GeSe. The carrier mobilities from optical phonon scattering are calculated by Eq. (2), which are presented in Table 3. Total mobility from the acoustic and optical phonons scattering can be calculated by the Equation of $\frac{1}{\mu} = \frac{1}{\mu_A} + \frac{1}{\mu_O}$ [18]. It is noted that the electron mobilities from optical phonon scattering is smaller than those from longitudinal acoustic phonon scattering. The hole mobility from longitudinal acoustic phonon scattering is smaller than those from optical phonon scattering. Therefore, optical phonon scattering plays a decisive role in electron mobility. Hole mobility is mainly determined by longitudinal acoustic phonon scattering. The result is in agreement with previous investigation on SnS and SnSe [11]. We find that the longitudinal acoustic phonon DPT model will overestimate the electron mobility. Similar behavior has been observed in previous studies [18,41].

3.1.3. Carrier mobility calculated from EPC matrix elements

To accurately calculate the intrinsic mobility in EPW code, the electron band structure and phonon dispersion need to be interpolated to a dense **k** and **q** grid. It is reported that the **k** points near the CBM for single valley semiconductors is densitied to accelerate the convergence of mobility [70]. However, it is observed from band structures of GeS and GeSe that there are several valleys in the conduction band and valence band. So, the study is carried out in a uniformly distributed **k** points samples, and randomly distributed **q** points samples. The detailed convergence test is shown in Fig. 8. The **k** points change in the range from 80 × 80 × 1 to 110 × 110 × 1 with an interval of 10 × 10 × 1 and the **q** points from 6000 to 12000 with an interval of 2000. The results show that the mobility change is less than 2% when the **q** points is larger than 8000 and the **k** points larger than 100 × 100 × 1. This is generally considered as the convergence standard for mobility calculation [41,45]. Therefore, the final set of **q** and **k** points is 8000 and 100 × 100 × 1, respectively. Table 4 shows the mobility at room temperature. For monolayer GeS (GeSe), the mobility of electrons is 7.01×10^1 cm^2 V^{-1} s^{-1} (1.33×10^2 cm^2 V^{-1} s^{-1}) along x direction, and 3.15×10^1 cm^2 V^{-1} s^{-1} (7.31×10^1 cm^2 V^{-1} s^{-1}) along y direction, respectively. The hole mobility is 5.93×10^1 cm^2 V^{-1} s^{-1} (3.43×10^2 cm^2 V^{-1} s^{-1}) along x direction, and 1.89×10^1 cm^2 V^{-1} s^{-1} (1.61×10^2 cm^2 V^{-1} s^{-1}) along y direction.

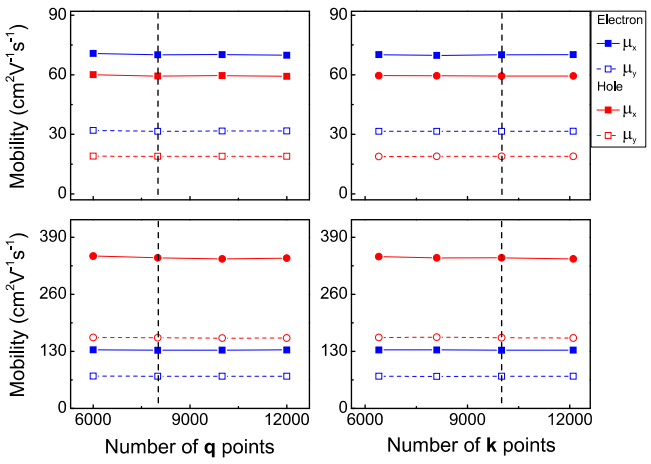

Fig. 8. At room temperature, the mobility depends on **q** and **k** points. In this study, a random **q** points in Brillouin zone change from 6000 to 12000 with an interval of 2000. A uniform **k** points from 80 × 80 × 1 to 110 × 110 × 1 with an interval of 10 × 10 × 1.

Table 4
At room temperature (T = 300 K), the mobility obtained from EPC matrix elements.

Materials	Carrier type	μ_x (cm^2 V^{-1} s^{-1})	μ_y (cm^2 V^{-1} s^{-1})
GeS	Electron	7.01×10^1	3.15×10^1
	Hole	5.93×10^1	1.89×10^1
GeSe	Electron	1.33×10^2	7.31×10^1
	Hole	3.43×10^2	1.61×10^2

The average velocity is calculated from [45]

$$\bar{v}(\epsilon) = \frac{\sum_{n\mathbf{k}} |v_{n\mathbf{k}}| \delta(\epsilon - \epsilon_{n\mathbf{k}})}{\sum_{n\mathbf{k}} \delta(\epsilon - \epsilon_{n\mathbf{k}})} \quad (4)$$

where $\epsilon_{n\mathbf{k}}$ represents the energy of carriers in the $n\mathbf{k}$ state. Fig. 9 shows the average velocity at different energy levels. It is noted that the average velocity of electrons and holes in the x direction are larger than those in the y direction. According to the mobility formula described in Eq. (3), carrier mobility is proportional to the square of velocity. Therefore, the higher mobility along x axis is related to the larger carrier velocity. The average hole velocity of GeS decreases sharply at about 0.1 eV. This is due to the appearance of another local valley VBM′ near VBM, which can be observed in Fig. 2. The average electron velocity of GeS decreases at about 0.18 eV, which corresponds to the local CBM′. For monolayer GeSe, the average electron velocity decreases sharply at about 0.02 eV and 0.16 eV, which corresponds to the local CBM′ and CBM″.

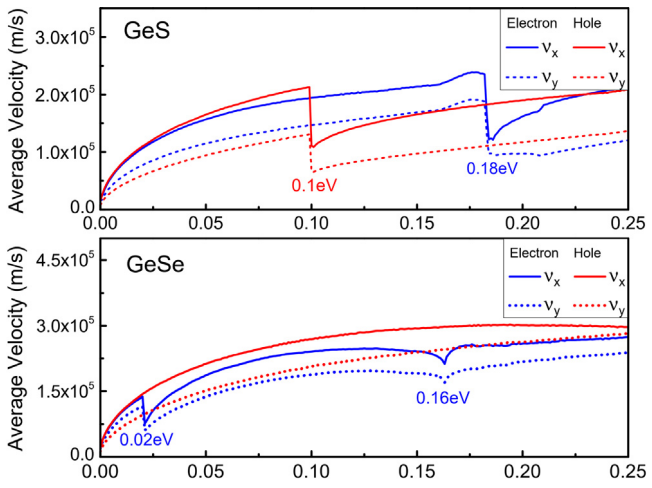

Fig. 9. The average velocities of electrons and holes at different energy levels.

Table 5
At room temperature (T = 300 K), the mobility obtained by calculating the EPC matrix element including polarization effect.

Materials	Carrier type	μ_x ($cm^2\ V^{-1}\ s^{-1}$)	μ_y ($cm^2\ V^{-1}\ s^{-1}$)
GeS	Electron	4.07×10^1	1.94×10^1
	Hole	4.77×10^1	1.52×10^1
GeSe	Electron	1.48×10^2	7.55×10^1
	Hole	2.47×10^2	1.16×10^2

Fig. 10 exhibits the distribution intensity of mobility in the whole Brillouin zone. It is observed that mobility in x direction is higher than that in y direction. For GeS, the main contribution to the electron and hole mobility is the carrier near CBM and VBM. The hole near VBM′ has a slight effect on the mobility along x direction. For GeSe, the electron mobility is determined by the CBM and CBM′, and hole mobility only dominated by the VBM.

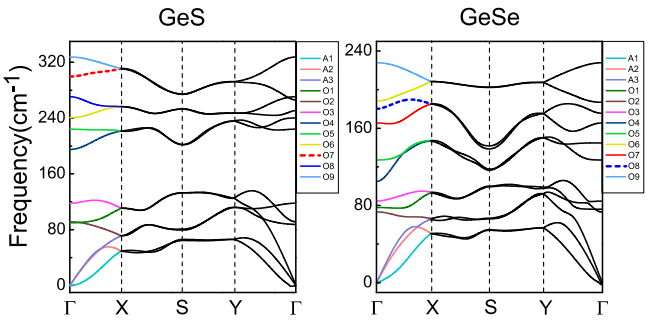

Fig. 11. Considering the phonon dispersion curve after polarization, the red solid line is a branch of the monolayer GeS change and the blue solid line is a branch of the monolayer GeSe change.

3.2. Carrier mobility with polarization effect from EPC matrix elements

In polar semiconductors, longitudinal optical phonon at long wavelength will generate an electric field, which couples with carrier [72]. These phonons are often called as polarized phonons (PPs). In the above calculation, we do not consider the polarization effect of semiconductors. If the polarization effect is not included in the calculation, the electron occupancy for self consistent field (SCF) calculation is employed by smearing method with 0.05 Ry broadening. If polarization effect is considered in the calculation, electron occupation will be fixed, the Born effective charge and dielectric constant are considered in the phonon dispersion [39,41].

Table 5 shows the mobility of carriers at 300 K. The electron mobilities for GeS (GeSe) are 4.07×10^1 $cm^2\ V^{-1}\ s^{-1}$ (1.48×10^2 $cm^2\ V^{-1}\ s^{-1}$) along x direction, and 1.94×10^1 $cm^2\ V^{-1}\ s^{-1}$ (7.55×10^1 $cm^2\ V^{-1}\ s^{-1}$) along y direction. The hole mobilities are 4.77×10^1 $cm^2\ V^{-1}\ s^{-1}$ (2.47×10^2 $cm^2\ V^{-1}\ s^{-1}$) along x direction, and 1.52×10^1 $cm^2\ V^{-1}\ s^{-1}$ (1.16×10^2 $cm^2\ V^{-1}\ s^{-1}$) along y direction. Compared with the previous results, the mobility of holes and electrons for GeS is reduced. For GeSe, hole mobility is decreased. Therefore, PPs play an important role in scattering carriers. Fig. 11 shows the phonon dispersion including polarization effect. Compared with Fig. 2, it is found that longitudinal optical modes of O7 (GeS) and O8 (GeSe) change greatly. Therefore, PPs generated by longitudinal optical mode plays a decisive role in mobility, which is in

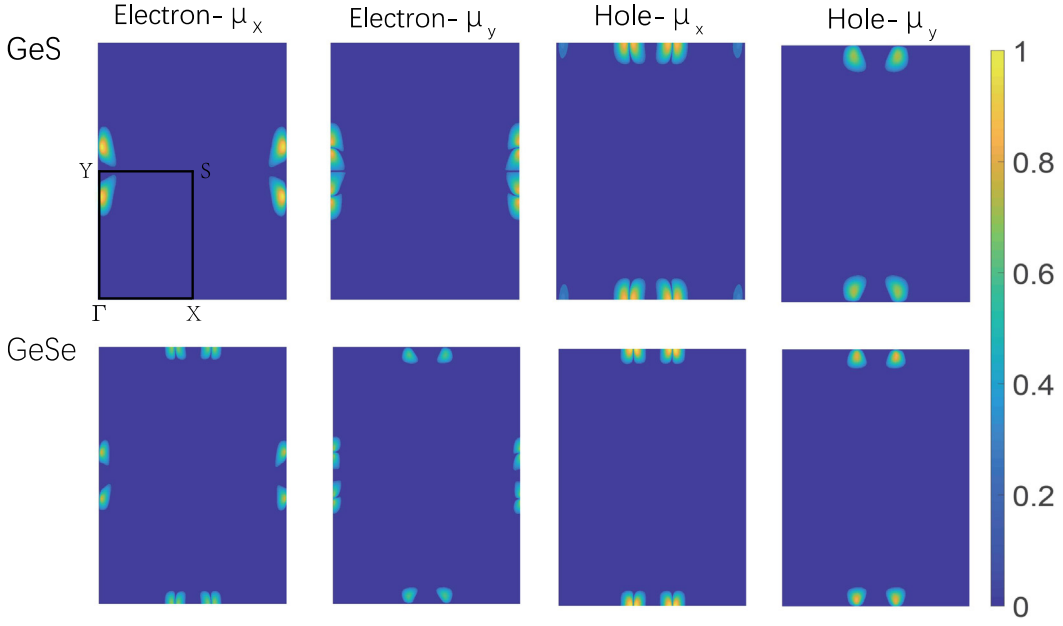

Fig. 10. Distribution intensity of mobility for monolayer GeS and GeSe in the whole Brillouin zone.

agreement with previous investigation [72]. For polar semiconductors, carrier will couple with longitudinal optical phonon at long wavelength limit, resulting in a Fröhlich interaction [37–39]. Compared with the above results, it is noted that the mobilities obtained from EPC matrix elements are smaller than those from longitudinal acoustic and optical phonon DPT models. Therefore, we verify that these empirical models may overestimate carrier mobility. Similar behaviors have also been observed in previous investigation [30,41,73]. The electron mobility of monolayer MoS_2 from longitudinal acoustic phonon DPT model is as high as 9.39×10^2 cm^2 V^{-1} s^{-1}, its value from the EPC matrix element is predicted to be only 3.95×10^2 cm^2 V^{-1} s^{-1} [41]. In addition, DPT theory predicts that mobility of monolayer BC_2N is as high as 5.26×10^4 cm^2 V^{-1} s^{-1} for electrons, and 1.48×10^4 cm^2 V^{-1} s^{-1} for hole [30]. The values from the EPC matrix element are only 5.84×10^1 cm^2 V^{-1} s^{-1} for electrons, and 4.14×10^1 cm^2 V^{-1} s^{-1} for hole.

4. Conclusions

In summary, carrier mobility of GeS (GeSe) is first investigated by DPT based on the density functional theory. At room temperature (T = 300 K), the value based on longitudinal acoustic phonon DPT is as high as 2.08×10^3 cm^2 V^{-1} s^{-1} (7.04×10^3 cm^2 V^{-1} s^{-1}) for electron, and 1.50×10^2 cm^2 V^{-1} s^{-1} (5.07×10^2 cm^2 V^{-1} s^{-1}) for hole. The mobility from optical phonon DPT is 3.89×10^2 cm^2 V^{-1} s^{-1} (5.06×10^2 cm^2 V^{-1} s^{-1}) for electron, and 5.57×10^2 cm^2 V^{-1} s^{-1} (2.62×10^3 cm^2 V^{-1} s^{-1}) for hole. The results show that the electron mobility is mainly determined by the optical phonon scattering, while the hole mobility is controlled by the longitudinal acoustic phonon scattering. Then, we accurately calculate the mobility from the EPC matrix elements. If the polarization effect is included in the calculation, the mobility is reduced to 4.07×10^1 cm^2 V^{-1} s^{-1} (1.48×10^2 cm^2 V^{-1} s^{-1}) for electron, and 4.77×10^1 cm^2 V^{-1} s^{-1} (2.47×10^2 cm^2 V^{-1} s^{-1}) for hole. We reveal that the longitudinal optical phonon plays a decisive role in carrier mobility. Comparing the results, it is found that the DPT will overestimate the carrier mobility. On the one hand, these empirical models usually only consider carrier scattered from a branch phonon. The contribution of other phonons to mobility is excluded from the calculation. On the other hand, PPs in polar semiconductors play an important role in mobility, which is also excluded in DPT model.

Declaration of competing interest

The authors declared that they have no conflicts of interest to this work.

CRediT authorship contribution statement

Mei Yang: Conceptualization, Methodology, Writing — original draft. **Shuo Cao:** Formal analysis. **Qi You:** Software. **Li-Bin Shi:** Investigation, Resources, Writing — review & editing. **Ping Qian:** Project administration, Funding acquisition.

Acknowledgments

This work was financially supported by the National Key Research and Development Program of China (Grant Nos. 2018YFB0704300 and 2016YFB0700500); the National Natural Science Foundation of China (No. 11847007) and Natural Science Foundation of Liaoning Province, China (No. 20180550566).

References

[1] B. Mortazavi, M. Shahrokhi, M. Raeisi, X. Zhuang, L.F.C. Pereira, T. Rabczuk, Carbon 149 (2019) 733–742.
[2] C. Tan, X. Cao, X.-J. Wu, Q. He, J. Yang, X. Zhang, J. Chen, W. Zhao, S. Han, G.-H. Nam, et al., Chem. Rev. 117 (2017) 6225–6331.
[3] J. Miao, S. Zhang, L. Cai, M. Scherr, C. Wang, ACS Nano 9 (2015) 9236–9243.
[4] B. Mortazavi, H. Yang, F. Mohebbi, G. Cuniberti, T. Rabczuk, Appl. Energy 202 (2017) 323–334.
[5] K.-C. Zhang, Y.-F. Li, Y. Liu, Y. Zhu, Carbon 102 (2016) 39–50.
[6] L.-B. Shi, Y.-Y. Zhang, X.-M. Xiu, H.-K. Dong, Carbon 134 (2018) 103–111.
[7] G. Schusteritsch, M. Uhrin, C.J. Pickard, Nano Lett. 16 (2016) 2975–2980.
[8] L.-B. Shi, S. Cao, J. Zhang, X.-M. Xiu, H.-K. Dong, Physica E 103 (2018) 252–263.
[9] Z. Li, J. Wang, Z. Liu, J. Chem. Phys. 141 (2014) 144107.
[10] L. Cheng, C. Zhang, Y. Liu, J. Am. Chem. Soc. (2019).
[11] L.-B. Shi, M. Yang, S. Cao, Q. You, Y.-Y. Niu, Y.-Z. Wang, Appl. Surf. Sci. (2019).
[12] E. Orestes, H.J. Freire, K. Capelle, Modern Aspects of Electrochemistry, No. 44, Springer, 2009, pp. 341–408.
[13] K.-C. Zhang, Y.-F. Li, Y. Liu, Y. Zhu, Phys. Chem. Chem. Phys. 20 (2018a) 28169–28175.
[14] H. Zhang, X. Zhang, G. Yang, X. Zhou, J. Phys. Chem. C 122 (2018b) 5291–5302.
[15] J. Shi, X. Zhao, Z. Wang, Y. Liu, Small (2019) 1901899.
[16] H. Sakaki, T. Noda, K. Hirakawa, M. Tanaka, T. Matsusue, Appl. Phys. Lett. 51 (1987) 1934–1936.
[17] F. Giustino, Rev. Modern Phys. 89 (2017) 015003.
[18] Z. Huang, W. Zhang, W. Zhang, Materials 9 (2016) 716.
[19] X. Zhao, Y. Ji, J. Chen, W. Fu, J. Dan, Y. Liu, S.J. Pennycook, W. Zhou, K.P. Loh, Adv. Mater. 31 (2019) 1900237.
[20] K.-C. Zhang, Y.-F. Li, Y. Liu, Y. Zhu, J. Phys.: Condens. Matter 31 (2018) 045802.
[21] H. Zhang, X. Li, X. Meng, S. Zhou, G. Yang, X. Zhou, J. Phys.: Condens. Matter 31 (2019a) 125301.
[22] K.-C. Zhang, Y.-F. Li, Y. Liu, Y. Zhu, J. Appl. Phys. 125 (2019b) 193903.
[23] B. Mortazavi, O. Rahaman, T. Rabczuk, L.F.C. Pereira, Carbon 106 (2016) 1–8.
[24] B. Mortazavi, M. Shahrokhi, A.V. Shapeev, T. Rabczuk, X. Zhuang, J. Mater. Chem. C 7 (2019) 10908–10917.
[25] T. Sohier, M. Calandra, C.-H. Park, N. Bonini, N. Marzari, F. Mauri, Phys. Rev. B 90 (2014) 125414.
[26] L.-B. Shi, S. Cao, M. Yang, Physica E 107 (2019) 124–130.
[27] T. Sohier, M. Calandra, F. Mauri, Phys. Rev. B 96 (2017a) 075448.
[28] T. Sohier, M. Gibertini, M. Calandra, F. Mauri, N. Marzari, Nano Lett. 17 (2017b) 3758–3763.
[29] H. Zhang, Y. Liao, G. Yang, X. Zhou, ACS Omega 3 (2018) 10517–10525.
[30] J. Xie, Z.Y. Zhang, D.Z. Yang, D.S. Xue, M.S. Si, J. Phys. Chem. Lett. 5 (2014) 4073–4077.
[31] J. Wang, R. Zhao, Z. Liu, Z. Liu, Small 9 (2013) 1373–1378.
[32] M.V. Fischetti, S.E. Laux, J. Appl. Phys. 80 (1996) 2234–2252.
[33] A. Shafique, A. Samad, Y.-H. Shin, Phys. Chem. Chem. Phys. 19 (2017) 20677–20683.
[34] M. Zhou, X. Chen, M. Li, A. Du, J. Mater. Chem. C 5 (2017) 1247–1254.
[35] I. Hase, H. Sugawara, H. Yoshizawa, H. Sato, J. Phys. Soc. Japan 75 (2006) 123602.
[36] Y.-C. Chang, R. James, Phys. Rev. B 55 (1997) 8219.
[37] H. Fröhlich, Adv. Phys. 3 (1954) 325–361.
[38] C. Verdi, F. Giustino, Phys. Rev. Lett. 115 (2015) 176401.
[39] J.-J. Zhou, M. Bernardi, Phys. Rev. B 94 (2016) 201201.
[40] Y. Liu, W. Wu, I.I.I. W. A. Goddard, J. Am. Chem. Soc. 140 (2018) 550–553.
[41] L. Cheng, Y. Liu, J. Am. Chem. Soc. 140 (2018) 17895–17900.
[42] A. Rodin, A. Carvalho, A.C. Neto, Phys. Rev. Lett. 112 (2014) 176801.
[43] L. Li, Y. Yu, G.J. Ye, Q. Ge, X. Ou, H. Wu, D. Feng, X.H. Chen, Y. Zhang, Nature Nanotechnol. 9 (2014) 372.
[44] X. Ling, H. Wang, S. Huang, F. Xia, M.S. Dresselhaus, Proc. Natl. Acad. Sci. 112 (2015) 4523–4530.
[45] J. Ma, Y. Chen, W. Li, Phys. Rev. B 97 (2018) 205207.
[46] D. Zhou, Q. Li, Y. Ma, Q. Cui, C. Chen, J. Phys. Chem. C 117 (2013) 5352–5357.
[47] S. Zhang, N. Wang, S. Liu, S. Huang, W. Zhou, B. Cai, M. Xie, Q. Yang, X. Chen, H. Zeng, Nanotechnology 27 (2016) 274001.
[48] E. Kress-Rogers, R. Nicholas, J. Portal, A. Chevy, Solid State Commun. 44 (1982) 379–383.
[49] S. Magorrian, V. Zólyomi, V. Fal'Ko, Phys. Rev. B 94 (2016) 245431.
[50] D.D. Vaughn, R.J. Patel, M.A. Hickner, R.E. Schaak, J. Am. Chem. Soc. 132 (2010) 15170–15172.
[51] P. Ramasamy, D. Kwak, D.-H. Lim, H.-S. Ra, J.-S. Lee, J. Mater. Chem. C 4 (2016) 479–485.
[52] K. Bhatia, G. Parthasarathy, E. Gopal, J. Phys. Chem. Solids 45 (1984) 1189–1194.
[53] R. Fei, W. Li, J. Li, L. Yang, Appl. Phys. Lett. 107 (2015) 173104.
[54] X. Zhou, X. Hu, B. Jin, J. Yu, K. Liu, H. Li, T. Zhai, Adv. Sci. 5 (2018) 1800478.
[55] C. x. Xia, J. Du, X. w. Huang, W. b. Xiao, W. q. Xiong, T. x. Wang, Z. m. Wei, Y. Jia, J. j. Shi, J. b. Li, Phys. Rev. B 97 (2018) 115416.
[56] D.-J. Xue, J. Tan, J.-S. Hu, W. Hu, Y.-G. Guo, L.-J. Wan, Adv. Mater. 24 (2012) 4528–4533.
[57] L.C. Gomes, P. Trevisanutto, A. Carvalho, A. Rodin, A.C. Neto, Phys. Rev. B 94 (2016) 155428.
[58] F. Li, X. Liu, Y. Wang, Y. Li, J. Mater. Chem. C 4 (2016) 2155–2159.
[59] X. Lv, W. Wei, Q. Sun, F. Li, B. Huang, Y. Dai, Appl. Catal. B 217 (2017) 275–284.

[60] Y. Xu, H. Zhang, H. Shao, G. Ni, J. Li, H. Lu, R. Zhang, B. Peng, Y. Zhu, H. Zhu, et al., Phys. Rev. B 96 (2017) 245421.
[61] G. Guo, G. Bi, Micro & Nano Lett. 13 (2018) 600–605.
[62] A. Shafique, Y.-H. Shin, Sci. Rep. 7 (2017) 506.
[63] P. Giannozzi, S. Baroni, N. Bonini, M. Calandra, R. Car, C. Cavazzoni, D. Ceresoli, G.L. Chiarotti, M. Cococcioni, I. Dabo, et al., J. Phys.: Condens. Matter 21 (2009) 395502.
[64] J.P. Perdew, J.A. Chevary, S.H. Vosko, K.A. Jackson, M.R. Pederson, D.J. Singh, C. Fiolhais, Phys. Rev. B 46 (1992) 6671.
[65] J.P. Perdew, K. Burke, M. Ernzerhof, Phys. Rev. Lett. 77 (1996) 3865.
[66] T. Grandke, L. Ley, Phys. Rev. B 16 (1977) 832.
[67] Y. Ye, Q. Guo, X. Liu, C. Liu, J. Wang, Y. Liu, J. Qiu, Chem. Mater. 29 (2017) 8361–8368.
[68] J. Bardeen, W. Shockley, Phys. Rev. 80 (1950) 72.
[69] H. Lang, S. Zhang, Z. Liu, Phys. Rev. B 94 (2016) 235306.
[70] S. Poncé, E.R. Margine, F. Giustino, Phys. Rev. B 97 (2018) 121201.
[71] J. Noffsinger, F. Giustino, B.D. Malone, C.-H. Park, S.G. Louie, M.L. Cohen, Comput. Phys. Comm. 181 (2010) 2140–2148.
[72] T. Sohier, M. Calandra, F. Mauri, Phys. Rev. B 94 (2016) 085415.
[73] L.-B. Shi, S. Cao, M. Yang, Q. You, K.-C. Zhang, Y. Bao, Y.-J. Zhang, Y.-Y. Niu, P. Qian, J. Phys.: Condens. Matter 32 (2020) 065306.